NeuroImage: Clinical 23 (2019) 101896

Contents lists available at ScienceDirect

NeuroImage: Clinical

journal homepage: www.elsevier.com/locate/ynicl

# Rapid myelin water imaging for the assessment of cervical spinal cord myelin damage

Adam V. Dvorak[a,d,*], Emil Ljungberg[b], Irene M. Vavasour[c], Hanwen Liu[a,d], Poljanka Johnson[a], Alexander Rauscher[a,c,e,j], John L.K. Kramer[d,f], Roger Tam[c,g], David K.B. Li[c,i,j], Cornelia Laule[a,c,d,h], Laura Barlow[c,j], Hannah Briemberg[i], Alex L. MacKay[a,c], Anthony Traboulsee[i], Piotr Kozlowski[a,c,d,j], Neil Cashman[i], Shannon H. Kolind[a,c,d,i]

[a] Physics and Astronomy, University of British Columbia, 6224 Agricultural Road, Vancouver, BC V6T 1Z1, Canada
[b] Department of Neuroimaging, Institute of Psychiatry, Psychology & Neuroscience, King's College London, De Crespigny Park PO89, London SE5 8AF, United Kingdom
[c] Radiology, University of British Columbia, 2775 Laurel Street, Vancouver, BC V5Z 1M9, Canada
[d] International Collaboration on Repair Discoveries, University of British Columbia, 818 West 10th Avenue, Vancouver, BC V5Z 1M9, Canada
[e] Pediatrics, University of British Columbia, 4480 Oak Street BC Children's Hospital Vancouver, BC V6H 3V4, Canada
[f] School of Kinesiology, University of British Columbia, 210-6081 University Boulevard, Vancouver, BC V6T 1Z1, Canada
[g] School of Biomedical Engineering, University of British Columbia, 2222 Health Sciences Mall, Vancouver, BC V6T 1Z3, Canada
[h] Pathology & Laboratory Medicine, University of British Columbia, 2211 Wesbrook Mall, Vancouver, BC V6T 2B5, Canada
[i] Medicine (Neurology), University of British Columbia, 2211 Wesbrook Mall, Vancouver, BC, V6T 2B5, Canada
[j] UBC MRI Research Centre, University of British Columbia, 2211 Wesbrook Mall, Vancouver, BC, V6T 2B5, Canada

ARTICLE INFO

*Keywords:*
Mri
Myelin water imaging
Diffusion tensor imaging
Quantitative $T_1$
Spinal cord

ABSTRACT

*Background:* Rapid myelin water imaging (MWI) using a combined gradient and spin echo (GRASE) sequence can produce myelin specific metrics for the human brain. Spinal cord MWI could be similarly useful, but technical challenges have hindered routine application. GRASE rapid MWI was recently successfully implemented for imaging of healthy cervical spinal cord and may complement other advanced imaging methods, such as diffusion tensor imaging (DTI) and quantitative $T_1$ ($qT_1$).

*Objective:* To demonstrate the feasibility of cervical cord GRASE rapid MWI in multiple sclerosis (MS), primary lateral sclerosis (PLS) and neuromyelitis optica spectrum disorder (NMO), with comparison to DTI and $qT_1$ metrics.

*Methods:* GRASE MWI, DTI and $qT_1$ data were acquired in 2 PLS, 1 relapsing-remitting MS (RRMS), 1 primary-progressive MS (PPMS) and 2 NMO subjects, as well as 6 age ( ± 3 yrs) and sex matched healthy controls (HC). Internal cord structure guided template registrations, used for region of interest (ROI) analysis. Z score maps were calculated for the difference between disease subject and mean HC metric values.

*Results:* PLS subjects had low myelin water fraction (MWF) in the lateral funiculi compared to HC. RRMS subject MWF was heterogeneous within the cord. The PPMS subject showed no trends in ROI results but had a region of low MWF Z score corresponding to a focal lesion. The NMO subject with a longitudinally extensive transverse myelitis lesion had low values for whole cord mean MWF of 12.8% compared to 24.3% (standard deviation 2.2%) for HC. The NMO subject without lesions also had low MWF compared to HC. DTI and $qT_1$ metrics showed similar trends, corroborating the MWF results and providing complementary information.

*Conclusion:* GRASE is sufficiently sensitive to detect decreased myelin within MS spinal cord plaques, NMO lesions, and PLS diffuse spinal cord injury. Decreased MWF in PLS is consistent with demyelination secondary to motor neuron degeneration. GRASE MWI is a feasible method for rapid assessment of myelin content in the cervical spinal cord and provides complementary information to that of DTI and $qT_1$ measures.

* Corresponding author at: Room M10 Purdy Pavilion, 2221 Wesbrook Mall, Vancouver, BC V6T 2B5, Canada.
*E-mail address:* adam.dvorak@ubc.ca (A.V. Dvorak).

https://doi.org/10.1016/j.nicl.2019.101896
Received 27 March 2019; Received in revised form 8 June 2019; Accepted 11 June 2019
Available online 17 June 2019

## 1. Introduction

Conventional magnetic resonance imaging (MRI) can detect changes in tissue structure caused by neurological diseases with relatively high sensitivity but is non-specific to the nature of the change. Quantitative MRI techniques provide objective metrics that may better reflect specific tissue properties and pathological alterations, such as demyelination.

Myelin water imaging (MWI) has demonstrated high specificity to myelin content (MacKay et al., 1994) with *post-mortem* validation (Kozlowski et al., 2008; Laule et al., 2008; Laule et al., 2006) and has been applied to demyelinating diseases like multiple sclerosis (MS) (Laule et al., 2004; MacKay et al., 2006; Oh et al., 2007; Vargas et al., 2015), amyotrophic lateral sclerosis (ALS) (Kolind et al., 2013) and neuromyelitis optica spectrum disorder (NMO) (Jeong et al., 2016; Jeong et al., 2017; Manogaran et al., 2016). MWI is based on the fact that the magnetic resonance signal from water within human brain or spinal cord tissue can be separated into multiple components distinguished by characteristic $T_2$ relaxation times: typically, ~20 ms for water trapped within myelin lipid bilayers (myelin water), ~80 ms for intra- and extra-cellular water, and ~2 s for cerebrospinal fluid (CSF) (MacKay et al., 1994; Whittall et al., 1997). MWI data is traditionally acquired using a multi-echo spin echo (MSE) sequence to obtain a multi-exponential $T_2$ decay curve, which is decomposed into a sum of mono-exponential decays to produce a $T_2$ distribution (MacKay et al., 1994). The myelin water fraction (MWF) is the fraction of the total water signal in the $T_2$ distribution that is attributed to myelin water.

While the majority of MWI work has been conducted in brain, some studies have also explored MWI in the spinal cord, where measurement of myelin can further improve the understanding and treatment of neurological diseases (Laule and MacKay, 2014; Wu et al., 2006; Kearney et al., 2015; Liu et al., 2017; Laule et al., 2010; Kolind et al., 2015; Combes et al., 2017; Martin et al., 2016). However, spinal cord imaging has several technical challenges which have hindered the wide-spread implementation of MWI, including motion, flow of cerebrospinal fluid, susceptibility artifacts, and the spinal cord's small cross-sectional area (Stroman et al., 2014). Spinal cord MWI using the MSE sequence requires long acquisition times (~20 mins (Laule et al., 2010; MacMillan et al., 2011)) that are not practical for future clinical use. To reduce scan time, a 3D multi-echo gradient and spin echo (GRASE) sequence for MWI has been proposed, which combines 2 gradient echoes with each spin echo to reduce acquisition time by a factor of 3. The 3D GRASE method has been validated in healthy control spinal cord to be in good agreement with the MSE sequence and highly reproducible, with an average coefficient of variation of 6.1% (Ljungberg et al., 2016). The 3D GRASE method has yet to be applied in disease.

Two additional quantitative MRI techniques that have been applied in spinal cord studies are diffusion tensor imaging (DTI) and quantitative $T_1$ mapping ($qT_1$). The fractional anisotropy (FA) and radial diffusivity (RD) metrics produced by DTI are affected by axonal degeneration and demyelination and are commonly used to provide insight into changes in tissue structure and integrity (Feldman et al., 2010). $qT_1$ values are also affected by multiple factors, such as water content and axonal size, but can provide a useful indicator of inflammatory pathological events (Harkins et al., 2016; Kolind and Deoni, 2011).

This study uses 3D GRASE MWI, alongside DTI and $qT_1$, in the cervical spinal cord of a diverse patient cohort. The primary goal was to demonstrate the feasibility of using this accelerated MWI sequence to measure the MWF in cervical spinal cords with disease.

## 2. Materials and methods

### 2.1. Participants

This study operated under ethics approval from the University of British Columbia Clinical Research and Ethics Board. All subjects signed consent forms prior to participation. The group of 6 participants with neurological diseases included 2 with primary lateral sclerosis (**PLS 1**: 44 year-old female, **PLS 2**: 64 year-old female); 1 with relapsing-remitting MS (**RRMS**: 30 year-old male with expanded disability status scale (EDSS (Kurtzke, 1983)) 2.0); 1 with primary progressive MS (**PPMS**: 53 year-old male with EDSS 6.0); and 2 with NMO (**NMO 1**: 37 year-old female with EDSS 2.0, **NMO 2**: 57 year-old female with EDSS 1.0). Only RRMS, PPMS, and NMO 1 had spinal cord lesions visible on $T_2$-weighted anatomical imaging. Imaging was also performed on 6 age ( ± 3 yrs) and sex matched healthy control subjects without a history of spinal cord disease or injury (4 females, 2 males, mean = 48 yrs., σ = 11 yrs., range 30-62 yrs.).

### 2.2. MRI

All imaging was performed at the UBC MRI Research Centre on a 3.0 T MRI scanner (Achieva, Philips Medical Systems, Best, The Netherlands) with a 6-channel spine coil. Axial scans were centered at the level of the C2/C3 disc and slices were aligned perpendicular to the cord, which provided full coverage of the C2 and C3 cord levels and partial coverage of C1 and C4. MWI data were acquired with the 3D GRASE sequence (Prasloski et al., 2012b) as adapted to cervical spinal cord by Ljungberg et al. (2016) to allow direct comparison with previous GRASE and MSE derived MWF values. $qT_1$ data were acquired using the driven-equilibrium single-pulse observation of $T_1$ method with flip angle correction (DESPOT1-HIFI) (Deoni, 2007). A high-resolution multi-echo gradient echo (mFFE) sequence was acquired for anatomical white/gray matter contrast, required for our analysis process. A sagittal $T_2$ weighted image was acquired for identification of lesions and other pathology. Imaging sequence details are outlined in Table 1. Note that data for NMO 2 was acquired as part of a separate study that did not include DTI or $qT_1$ data.

### 2.3. Data analysis

GRASE MWF maps were produced in-house using a regularized non-negative least-squares fitting algorithm with stimulated echo correction (Prasloski et al., 2012a; Yoo et al., 2015). $T_2$ relaxation times between 15 ms and 40 ms were associated with myelin water (Laule et al., 2010). The Spinal Cord Toolbox software was used for DTI motion correction and calculation of FA and RD metrics (De Leener et al., 2017). $qT_1$ maps were calculated using Quantitative Imaging Tools (QUIT) software (Wood, 2018).

A segmentation and registration pipeline was built using Spinal Cord Toolbox [23] to perform region of interest (ROI) analysis and create Z score maps. A two-step process was developed for registration of the mFFE to the PAM50 template (De Leener et al., 2018). An initial registration combined rigid, slice-wise centre of mass rotation and affine algorithms to align the mFFE to the template. For the next step, we identified the C2 and C3 vertebral levels and manually segmented the gray matter on each slice of the mFFE. For subjects with cord lesions, segmentation was performed for all slices where gray matter was fully visible, then used to help estimate (visually interpolate) the segmentation for remaining slices where it was partially or fully obscured by lesion tissue. This anatomical information was used for a second registration between the mFFE and template, with slice-wise centre of mass rotation, non-linear symmetric normalization and B-spline regularized non-linear symmetric normalization. The two registrations were then concatenated to create a single warpfield (and its inverse) for warping between the PAM50 template and mFFE image spaces.

A warpfield for transforming between the PAM50 template and quantitative MRI image space was created by concatenating with the results of a rigid registration between the mFFE and quantitative MRI. For ROI analysis, probabilistic PAM50 template ROI were warped to the quantitative MRI space and thresholded to only include voxels with probability > 0.5 to reduce partial volume effects. ROI values were

**Table 1**
Anatomical and quantitative MRI acquisition details. Axial scans were centered at the level of the C2/C3 disc, which provided full coverage of the C2 and C3 cord levels and partial coverage of C1 and C4. Resolution (RES) and field of view (FOV) values correspond to the Left-Right, Ventral-Dorsal, and Inferior-Superior directions. (TE = Echo time, TR = Repetition time, TSE = Turbo spin echo, FA = Flip angle, SENSE = Sensitivity encoding).

| Anatomical | Quantitative | |
|---|---|---|
| **Sagittal $T_2$ -Weighted**<br>• 2D Multi-slice<br>• TR/TE: 3000/120 ms<br>• TSE Factor: 24<br>• FA: 90°<br>• RES: 0.8x1x3mm<br>• FOV: 160x250x36 mm<br>• Time: 3 min | **Myelin Water Imaging**<br>**3D Multi-echo Gradient and Spin Echo (GRASE)**<br>• Axial orientation, 16 slices<br>• 32 Echoes<br>• TR/TE: 1500/10 ms<br>• RES: 0.75x0.75x5mm<br>• FOV: 180x150x40mm<br>• Time: 8 min 36 s | **Quantitative $T_1$**<br>**3D Spoiled Gradient Recalled**<br>• Axial orientation, 14 slices<br>• TR/TE: 5.5/2.7 ms<br>• SENSE Factor: 2<br>• FA: 2,3,4,6,8,13,18°<br>• RES: 0.75x0.75x4 mm<br>• FOV: 180x200x56 mm<br>• Time: 7x11 s = 1 min 17s |
| **Multi-Echo Gradient Echo**<br>• 2D Multi-slice<br>• Axial orientation, 16 slices<br>• TR/TE1/TE2–5: 815/6.6/8.2 ms<br>• RES: 0.8x0.8x2.5 mm<br>• FOV: 150x150x43.75 mm<br>• Time: 5 min | **Diffusion Tensor Imaging**<br>• Axial orientation, 10 slices<br>• B-values: 0 & 750<br>• 32 directions<br>• TR/TE = 3362/68 ms<br>• RES:1x1x5mm<br>• FOV: 64x64x52mm<br>• Time: 4 min 42 s | **Quantitative $T_1$**<br>**3D Inversion Recovery Spoiled Gradient Recalled**<br>• Axial orientation, 14 slices<br>• TR/TE/TI: 5.5/2.7/350 ms<br>• SENSE Factor: 2<br>• FA: 5°<br>• RES: 0.75x0.8x8mm<br>• FOV: 180x200x56 mm<br>• Time: 17 s |

calculated using a weighted mean of the remaining voxels, where the quantitative MRI value of each voxel was weighted by its ROI probability. ROIs included the whole cord (WC), white matter (WM), gray matter (GM), dorsal column (DC) and lateral funiculi (LF).

Z score maps were created by warping individual quantitative maps from all subjects to template space, then calculating the sample mean ($\acute{x}$) and sample standard deviation (σ) of the healthy control subjects. Z score maps were calculated for each metric, where

$$Z = \frac{(x_{patient} - \acute{x})}{\sigma}$$

The maps were thresholded to exclude voxels with a coefficient of variation ($COV$) $> 0.7$ to correct for small sample size, where

$$COV = \left(1 + \frac{1}{4n}\right)\frac{\sigma}{\acute{x}}$$

and $n = 6$ for the 6 healthy controls. Most voxels excluded by the COV threshold (10% of MWF voxels, 11% of RD, 0% of FA, 2% of $qT_1$) were near the cord/CSF boundary. Due to variable cord coverage between subjects, axial views were produced by averaging only the slices in template space that contained all subjects (55 for GRASE, 45 for DTI, 50 for $qT_1$). Sagittal views were taken from a single representative, medial slice. The Z score maps were displayed using a diverging colour map, designed to be perceptually linear (Moreland, 2009).

The small sample size of each patient group limited possible statistical analyses, so instead we present an illustrative approach to the results; highlighting trends in ROI results for mean values at least 1σ larger or smaller than healthy control mean, and qualitatively examining Z score maps. Z score maps were scaled to Z = ± 2 for MWF and Z = ± 4 for DTI and $qT_1$ metrics.

## 3. Results

Fig. 2 shows raw MWF, RD, FA and $qT_1$ metric maps for all subjects, which were taken from a single representative slice at the C2/C3 disc level (the same slice for RD and FA) and masked to the spinal cord.

### 3.1. ROI results

ROI analysis results for MWF, RD, FA and $qT_1$ are presented in Table 2. Both PLS subjects had low LF MWF, high GM RD, low WC, GM and LF FA, and low DC $qT_1$. PLS 1 had low FA in all ROIs. RRMS RD and $qT_1$ values were low in WC, WM, and DC, but high in GM. PPMS ROI results did not show any clear trends. NMO 1 had a longitudinally extensive transverse myelitis lesion at the C2/C3 level of the spinal cord (Fig. 1). NMO 1 MWF and FA metrics were low in all ROIs, RD was high in all ROIs, and $qT_1$ was high in all ROIs except LF. NMO 2 (without visible lesions) had low MWF values in all ROIs compared to HC. The visible outline of gray matter in the raw MWF and FA maps (Fig. 2) is in line with the consistently lower MWF and FA values in the GM ROI compared to WM.

### 3.2. Z score map results

MWF, RD, FA and $qT_1$ Z score maps are presented in Figs. 3, 4, 5 and 6, respectively. Both PLS subjects' Z score maps showed evidence of differences in quantitative MRI parameters compared to the healthy control atlas. Z scores for MWF and FA appeared low while those for RD and $qT_1$ appeared high. These effects are more diffuse throughout the whole cord of PLS 1 and relatively focal to the lateral motor tracts for PLS 2.

RRMS and PPMS maps did not show clear trends in axial view, however Fig. 3 shows that a cord lesion visible on an axial slice of the anatomical image corresponds to a region of low MWF Z score at the exact same level of the sagittal view.

NMO 1 Z scores were very low for MWF and FA and very high for RD and $qT_1$. This trend held throughout the superior-inferior direction of the entire imaging volume, as shown in the sagittal view in Fig. 3. NMO 2 (without visible lesions) had low MWF Z score spread diffusely throughout the cord. Comparison of raw metric maps between subjects in Fig. 2 shows qualitative agreement with the trends suggested by Z score maps.

## 4. Discussion

### 4.1. Utility of GRASE MWI in cervical spinal cord

The MWF values for healthy controls (whole cord mean = 24.3%, σ = 2.2%) were in good agreement with the results from another healthy control cohort (mean 22.9%, σ = 2.5%) (Ljungberg et al., 2016) and compared to the traditional MSE sequence (22.5%, σ = 3.4% and 24.9% σ = 4.2%) (Wu et al., 2006; Minty et al., 2009; Laule et al.,

**Table 2**
Mean values within each specified ROI for healthy control (HC), primary lateral sclerosis (PLS), relapsing-remitting and primary-progressive multiple sclerosis (RRMS, PPMS) and neuromyelitis optica spectrum disorder subjects with (NMO 1) and without (NMO 2) a visible transverse myelitis spinal cord lesion. Values that differ from HC mean by $\geq 1\sigma$ or $\leq -1\sigma$ are **bold** for emphasis, values that differ by $\geq 2\ \sigma$ or $\leq -2\ \sigma$ are **bold***.

| | **Myelin Water Fraction (%)** | | | | | **Radial Diffusivity ($10^{-3} \cdot mm^2 \cdot s^{-1}$)** | | | | |
|---|---|---|---|---|---|---|---|---|---|---|
| | Whole Cord | White Matter | Gray Matter | Dorsal Column | Lateral Funiculi | Whole Cord | White Matter | Gray Matter | Dorsal Column | Lateral Funiculi |
| HC (σ) | 24.3 (2.2) | 26.3 (2.1) | 16.8 (2.4) | 28.1 (2.8) | 25.2 (1.9) | 0.602 (0.080) | 0.614 (0.095) | 0.552 (0.022) | 0.609 (0.084) | 0.572 (0.110) |
| PLS 1 | 22.5 | 24.8 | **13.5** | 28.8 | **22.5** | 0.672 | 0.660 | **0.728*** | 0.667 | 0.638 |
| PLS 2 | 24.4 | 27.0 | 16.7 | **31.4** | **22.1** | 0.630 | 0.626 | **0.643*** | 0.618 | 0.612 |
| RRMS | 24.4 | 25.9 | 17.5 | **31.0** | **23.1** | **0.503** | **0.486** | **0.589*** | **0.485** | 0.496 |
| PPMS | 25.1 | 27.4 | 16.8 | 29.3 | 25.5 | 0.533 | 0.541 | **0.500** | 0.614 | 0.494 |
| NMO 1 (lesion) | **12.8*** | **14.0*** | **6.3*** | **6.9*** | **16.0*** | **0.962*** | **0.970*** | **0.917*** | **1.083*** | **0.904*** |
| NMO 2 (no lesion) | **20.5** | **22.2** | **11.3*** | **22.2*** | **23.1** | — | — | — | — | — |

| | **Fractional Anisotropy (%)** | | | | | **Mean $T_1$ ($ms$)** | | | | |
|---|---|---|---|---|---|---|---|---|---|---|
| | Whole Cord | White Matter | Gray Matter | Dorsal Column | Lateral Funiculi | Whole Cord | White Matter | Gray Matter | Dorsal Column | Lateral Funiculi |
| HC (σ) | 69.1 (3.5) | 70.7 (3.7) | 61.6 (2.4) | 70.8 (3.5) | 72.0 (3.6) | 982 (36) | 994 (44) | 937 (31) | 944 (65) | 981 (60) |
| PLS 1 | **59.5*** | **62.2*** | **46.2*** | **61.5*** | **62.8*** | **939** | **937** | 946 | **863** | 932 |
| PLS 2 | **64.7** | 67.2 | **56.9** | 69.5 | **66.0** | 975 | 974 | **979** | **859** | **1050** |
| RRMS | 70.4 | 72.4 | 60.6 | **74.6** | 71.0 | **938** | **925** | **1011*** | **863** | 945 |
| PPMS | 72.0 | 72.9 | **67.8*** | 72.1 | 72.5 | **931** | **925** | 950 | 922 | 928 |
| NMO 1 (lesion) | **45.6*** | **46.7*** | **39.8*** | **43.8*** | **47.9*** | **1109*** | **1078** | **1308*** | **1218*** | 1033 |

2010; MacMillan et al., 2011).

Identifying subtle abnormalities in normal-appearing spinal cord on an individual level is difficult due to heterogeneity between individuals and limitations in the sensitivity of advanced MRI metrics. This difficulty can be accentuated by ROI analyses of quantitative MRI metrics, which can obscure evidence of pathology by averaging across heterogeneous tissue. Z score maps can provide a more complete representation of quantitative metric results by depicting voxel-wise magnitudes of tissue change relative to a healthy control population. The GRASE MWI sequence reduces acquisition time compared to previous $T_2$ relaxation methods and should be practical and useful in larger cohorts or longitudinal studies of focal and diffuse spinal cord involvement in demyelinating diseases.

### 4.2. Primary lateral sclerosis

The Pringle criteria, developed in 1992 for clinical diagnosis of PLS, describes a motor neuron disease causing degeneration of upper motor neurons (Pringle et al., 1992). This differs from the more common, faster progressing ALS, which affects both upper and lower motor neurons. Both diseases present with axonal degeneration in the motor cortex of the brain, which causes Wallerian degeneration along the distal portion of the axon, leading to subsequent degradation of the myelin sheath. This should be visible as demyelination of the corticospinal tracts, which extend from the motor cortex of the brain to the lower motor neurons in the spinal cord.

MRI studies of ALS, and the rarer PLS, have found that DTI metrics are sensitive to pathological changes invisible to conventional MRI (Wang et al., 2014; Simon et al., 2014; Muller et al., 2018) and that FA could potentially be used as a biomarker for progression of upper motor neuron degeneration (Nickerson et al., 2009). Significantly low FA has been found in ALS cervical spinal cord compared to healthy controls (Nair et al., 2010; Agosta et al., 2009; Wang et al., 2014), and correlated significantly with functional testing (Nair et al., 2010). Wang et al. found low FA focal to the lateral corticospinal tracts of ALS cord (Wang et al., 2014). These previous studies are in line with our findings; both PLS subjects had low MWF in the lateral funiculi ROI of the cord, providing evidence of demyelination in the descending motor fibers of the corticospinal tract. FA values are less specific to demyelination, but low FA in the lateral funiculi support the MWF results.

MRI studies in ALS also show that DTI metrics can detect presymptomatic axonal degeneration (Gatto, 2018). GRASE MWI could be coupled with DTI to improve characterisation of motor neuron disease effects on the spinal cord, as done previously to study microstructural brain changes related to age (Billiet et al., 2015). Characterizing differences in spinal cord pathology for PLS (non-local Wallerian degeneration) and ALS (direct lower motor neuron degeneration) using quantitative MRI metrics could accelerate diagnosis of PLS, which is predicated on the exclusion of other candidate motor neuron diseases and often takes more than four years after symptom onset.

### 4.3. Multiple sclerosis

In MS, the early predominant features are focal regions of pathology. Quantitative MRI studies of MS brain generally segment this lesional tissue, allowing MRI metrics to be analyzed in better context with the disease (Faizy et al., 2016). This is technically difficult to perform in spinal cord, but higher resolution anatomical imaging, better lesion contrast (as available at higher field strength (Barry et al., 2018)), and increased availability of automated lesion segmentation tools (Gros et al., 2019) could facilitate such practice in future MRI studies of spinal cord.

Developing biomarkers for disease progression in spinal cord is valuable for many diseases but is especially crucial for improving understanding and treatment of the primary-progressive MS phenotype, which shows stronger correlations between clinical and radiological assessments in spinal cord than brain (Nijeholt et al., 1998). Several previous studies have successfully applied the MSE MWI method to an MS population, including a pilot study by Wu et al. which found low MWF in $T_2$-visible spinal cord lesions of MS patients (Wu et al., 2006) and Laule et al. who found a significant reduction in PPMS MWF over 2 years (10.5%, $p = 0.01$) (Laule et al., 2010).

Our results show a focal lesion that was hypo-intense (*i.e.* demyelinated) within the PPMS subject MWF Z score map (Fig. 3). No evidence of changes to normal-appearing (non-lesional) white matter were found for PPMS or RRMS, possibly due to limited statistical power from the small healthy control group. The RRMS subject had high MWF in the DC, corroborated by high FA in the same ROI. This may be because

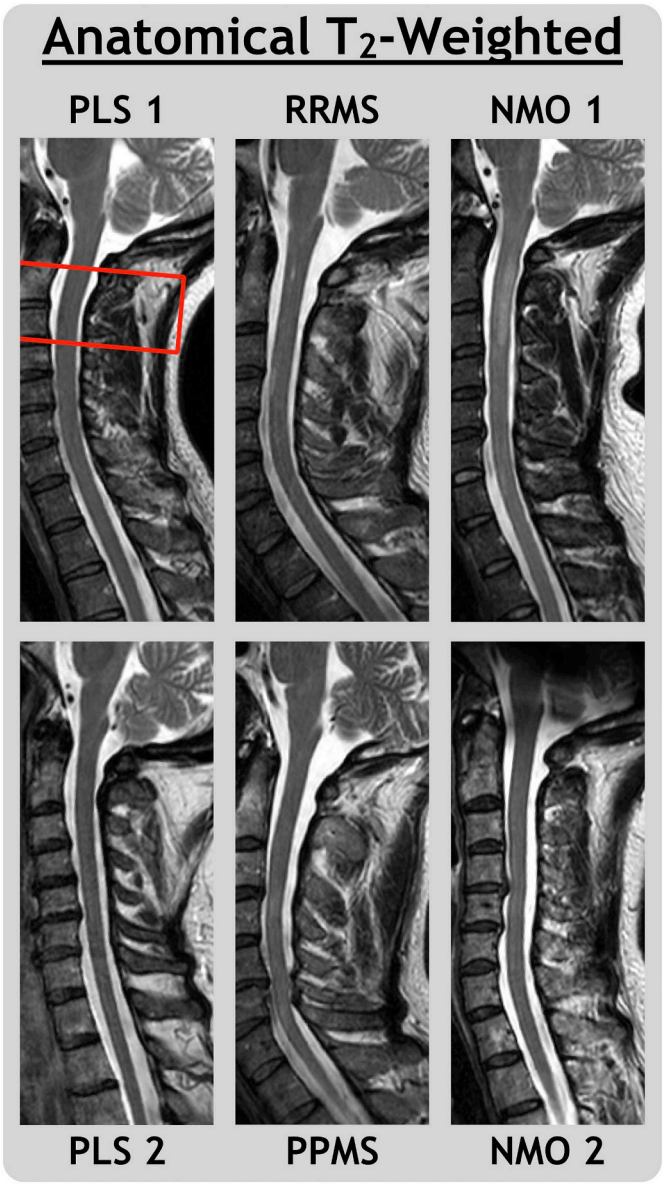


**Fig. 1.** Sagittal $T_2$-weighted MRI for primary lateral sclerosis (PLS), relapsing-remitting and primary-progressive multiple sclerosis (RRMS, PPMS) and neuromyelitis optica spectrum disorder subjects with (NMO 1) and without (NMO 2) a visible transverse myelitis spinal cord lesion. The quantitative MRI field of view is outlined for PLS 1.

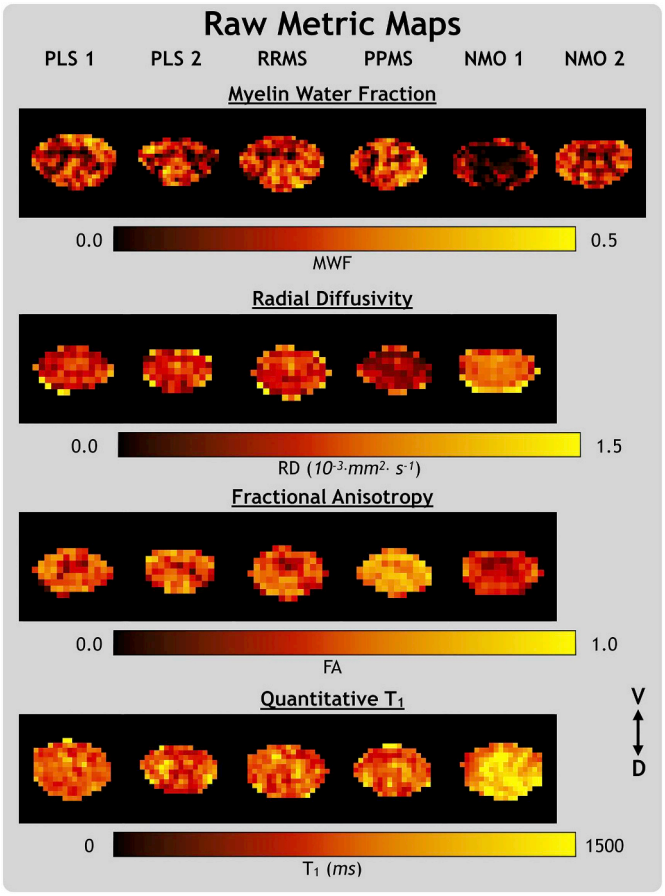


**Fig. 2.** Metric maps for the myelin water fraction (MWF), radial diffusivity (RD), fractional anisotropy (FA), and quantitative $T_1$ metrics in their native space. From left to right, the subjects are primary lateral sclerosis (PLS), relapsing-remitting and primary-progressive multiple sclerosis (RRMS, PPMS) and neuromyelitis optica spectrum disorder with (NMO 1) and without (NMO 2) a visible transverse myelitis spinal cord lesion. The ventral (V) and dorsal (D) anatomical directions are labelled.

the control group, with a mean age of 48 years, is not well representative of the 30 year-old RRMS subject and is expected to show increased evidence of age-related demyelination. PPMS and RRMS MWF Z score maps both show a qualitatively high degree of heterogeneity, with clusters of voxels nearing Z scores of $+2$ and $-2$. This could be related to the significant correlation between MS patient disability (EDSS score) and variance of brain MWF values in normal-appearing white matter, found in a previous study (Kolind et al., 2012a).

### 4.4. Neuromyelitis optica spectrum disorder

Previous studies of NMO have reported widespread changes in non-lesional spinal cord tissue (Qian et al., 2011; Jeantroux et al., 2012; Rivero et al., 2014; Pessoa et al., 2012). These could be due to non-local effects such as Wallerian degeneration, an interpretation supported by studies showing that NMO cord lesions affect DTI metrics much more drastically than MS lesions (Klawiter et al., 2012; Rivero et al., 2014). Combes et al. found short term changes in cervical cord tissue between relapses for MS but not NMO, further suggesting that diffuse NMO cord pathology is residual damage caused by a previous relapse (Combes et al., 2017). Alternatively, NMO could possess slow, diffuse inflammatory effects in the spinal cord that have not yet been well identified.

In our study, the $T_2$-weighted image of NMO 1 (Fig. 1) depicts a hyperintensity with characteristic signs of a longitudinally extensive transverse myelitis lesion; it covers most of the cross-sectional area of the cord, favouring gray matter (Nakamura et al., 2008; Krampla et al., 2009), and extends across 3 vertebral levels, from C1 to C3 (Wingerchuk et al., 1999). Our results, with low MWF and FA values in addition to high RD and $qT_1$ values, are indicative of the pathological changes expected within such a lesion. Low MWF values for NMO 2 agrees with the previous literature finding of change in the normal-appearing white matter of NMO cervical cord.

### 4.5. Limitations and future work

Our study is limited by the small sample size and diverse patient cohort, which renders statistical analyses impossible and limits quantitative interpretation of the Z score maps. Although the results would be more statistically striking with a homogeneous patient population, the goal of this study is rather to demonstrate the breadth of applications where GRASE is technically feasible for detecting differences in

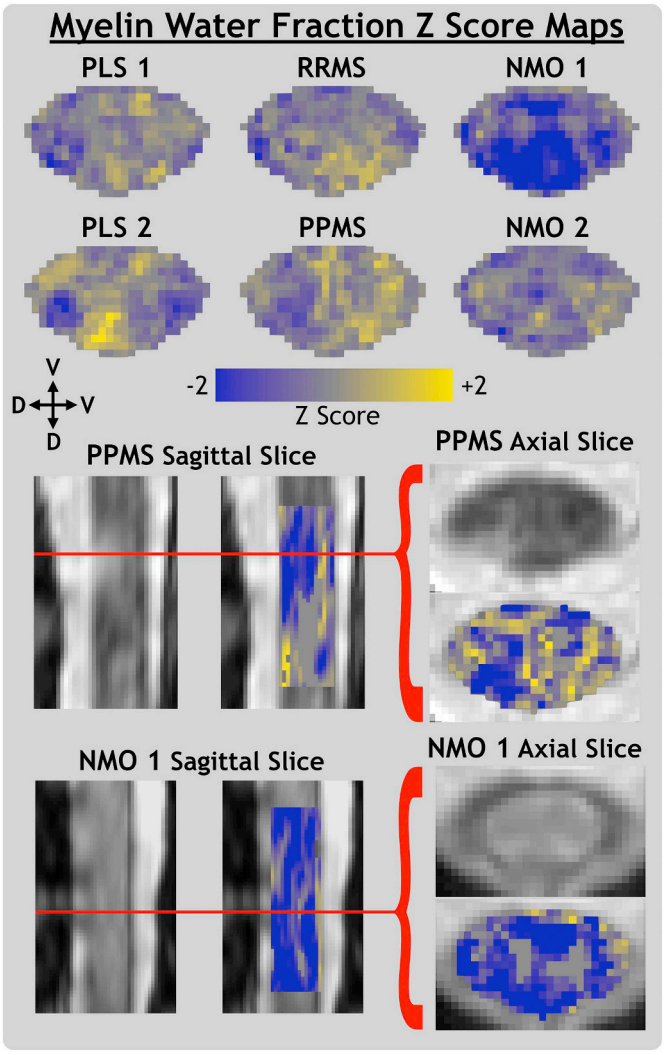


**Fig. 3.** Myelin water fraction Z score maps for primary lateral sclerosis (PLS), relapsing-remitting and primary-progressive multiple sclerosis (RRMS, PPMS) and neuromyelitis optica spectrum disorder subjects with (NMO 1) and without (NMO 2) a visible transverse myelitis spinal cord lesion. Individual slices of PPMS and NMO 1 anatomical MRI are shown in template space with Z score map slices superimposed. The ventral (V) and dorsal (D) anatomical directions are labelled for axial and sagittal views.

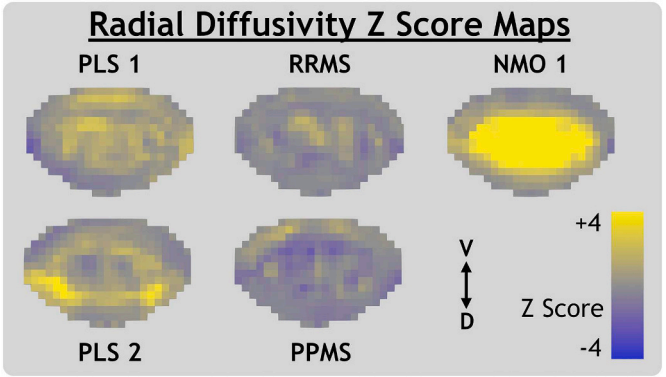


**Fig. 4.** Radial diffusivity Z score maps for primary lateral sclerosis (PLS), relapsing-remitting and primary-progressive multiple sclerosis (RRMS, PPMS) and neuromyelitis optica spectrum disorder with a visible transverse myelitis spinal cord lesion (NMO 1). The ventral (V) and dorsal (D) anatomical directions are labelled.

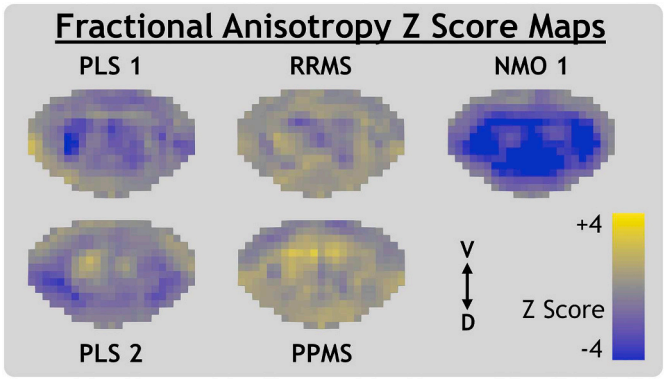


**Fig. 5.** Fractional anisotropy Z score maps for primary lateral sclerosis (PLS), relapsing-remitting and primary-progressive multiple sclerosis (RRMS, PPMS) and neuromyelitis optica spectrum disorder with a visible transverse myelitis spinal cord lesion (NMO 1). The ventral (V) and dorsal (D) anatomical directions are labelled.

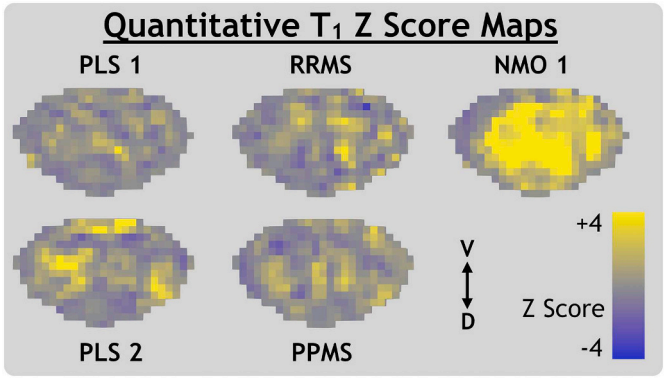


**Fig. 6.** Quantitative $T_1$ Z score maps for primary lateral sclerosis (PLS), relapsing-remitting and primary-progressive multiple sclerosis (RRMS, PPMS) and neuromyelitis optica spectrum disorder with a visible transverse myelitis spinal cord lesion (NMO 1). The ventral (V) and dorsal (D) anatomical directions are labelled.

spinal cord myelin content. We have demonstrated cases where demyelination is (1) expected (NMO lesions), (2) variable and requiring greater specificity than that provided by conventional MRI (MS cord plaques and normal-appearing white matter) and (3) secondary to defining disease characteristics and thus understudied (such as the low myelin measurements in PLS motor tracts, consistent with demyelination secondary to motor neuron degeneration). Future cross-sectional studies with larger, more uniform subject groups could refine our understanding of differences between diseased and healthy spinal cords on a group level.

However, our results demonstrate the ability to use MWF Z score maps to assess changes in cord myelin content within individual lesions or in normal-appearing white matter. The volume of brain with low MWF compared to healthy controls for an individual PPMS patient has been shown to correlate with clinical disability scores ($p = 0.008$, $R = 0.58$) (Kolind et al., 2012). Future MWI studies should extend this investigation to include spinal cord MWF values. Coupling these techniques with longitudinal data acquisition would quantify both temporal and spatial differences in myelin content, providing a more complete evaluation of disease progression or even treatment response. Future studies with frequent, longitudinal data acquisition could validate the reproducibility of using of spinal cord MWF Z score maps for monitoring individual patients.

Presenting the average of many Z score map slices creates more representative images but does not account for the natural differences in gray matter shape and myelin content at different cord levels.

Similarly, ROI analysis results do not necessarily reflect the heterogeneity or asymmetry of disease pathology within the ROI. Development and validation of automated spinal cord lesion segmentation tools would allow ROI results to be better interpreted in the context of pathology, by distinguishing between lesional and non-lesional tissue (Gros et al., 2019). Lesions can also obscure anatomical details of the gray matter structure, reducing the accuracy of template registrations. In the present study, gray matter for PPMS and RRMS subjects was only partially obscured (by lesions visible on 3 or fewer adjacent slices). NMO 1 gray matter was more significantly obscured, by the longitudinally extensive lesion visible on the majority of slices. This reduced the accuracy of the gray matter segmentation (and the anatomical alignment of intra-cord structures) for NMO 1. However, the gray matter segmentation could not have caused or significantly affected the evidence of diffuse pathology visible on NMO 1 Z score maps because the whole cord segmentation (overall cord alignment) was unaffected.

Control MWF had higher COV than the DTI and $qT_1$ metrics, which is why Z score maps were scaled between $Z = \pm 2$ for MWF and $Z = \pm 4$ for DTI and $qT_1$ metrics. This could be due to noise in the MWF values caused by the low signal from the short $T_2$ (myelin water) component, or because of greater natural variability in MWF than DTI or $qT_1$ metrics. DTI metrics provide greater sensitivity to pathology than MWF in our results, likely because DTI metrics are influenced by many tissue changes, such as edema, cellularity, axonal integrity and demyelination. The advantage of the MWF metric is not high sensitivity to regions of pathology, which can be provided by conventional MRI sequences, but rather the high specificity to myelin content. A multimodal quantitative MRI approach is ideal because combined results can provide complementary information. For example, in a region with low FA values, normal MWF values would suggest that FA changes are driven by factors other than demyelination.

Future study adapting GRASE MWI to cover the entire cervical spinal cord, or even thoracic cord, could provide more insight into the spatial variation of myelin along the cord. This would be especially useful for the study of motor neuron disease, such as ALS (where more extreme changes in DTI metrics are found in the distal cervical spinal cord (Nair et al., 2010)), and for imaging at the site of low-level spinal cord injury.

## 5. Conclusions

Our study acquired independent DTI and quantitative $T_1$ metrics in conjunction with GRASE MWI to corroborate evidence of pathology from the MWF results. MWF values reflected our expectations, showing: agreement with the previous implementation of GRASE MWI in healthy controls, changes in myelin content expected with PLS, and marked sensitivity to lesions in MS and NMO subjects. In addition to providing pilot data, this study demonstrates the ability to measure the MWF metric, a biomarker with high specificity to myelin, in the cervical spinal cord of disease patients with a clinically feasible acquisition time (8.5 min).

## Acknowledgements

We thank all of the participants in this study, Dayna Ortner for coordinating recruitment and logistics of this study, the UBC MRI Research Centre and its MRI technologists, and the neurologists who recruited participants.

This work was supported by a Natural Sciences and Engineering Research Council of Canada (NSERC) Discovery Grant [F17-05113]. Shannon Kolind is supported by the Milan & Maureen Ilich Foundation as well as the Michael Smith Foundation for Health Research (Scholar Award). Emil Ljungberg is in receipt of a PhD studentship jointly funded by General Electric (GE) Healthcare and the National Institute for Health Research (NIHR) Biomedical Research Centre at South London and Maudsley NHS Foundation Trust and King's College London.

## References

Agosta, F., Rocca, M.A., Valsasina, P., Sala, S., Caputo, D., Perini, M., Salvi, F., Prelle, A., Filippi, M., 2009. A longitudinal diffusion tensor MRI study of the cervical cord and brain in amyotrophic lateral sclerosis patients. J. Neurol. Neurosurg. Psychiatry 80, 53–55.

Barry, R.L., Vannesjo, S.J., By, S., Gore, J.C., Smith, S.A., 2018. Spinal cord MRI at 7T. Neuroimage 168, 437–451.

Billiet, T., Vandenbulcke, M., Madler, B., Peeters, R., Dhollander, T., Zhang, H., Deprez, S., Van den Bergh, B.R.H., Sunaert, S., Emsell, L., 2015. Age-related microstructural differences quantified using myelin water imaging and advanced diffusion MRI. Neurobiol. Aging 36, 2107–2121.

Combes, A.J.E., Matthews, L., Lee, J.S., Li, D.K.B., Carruthers, R., Traboulsee, A.L., Barker, G.J., Palace, J., Kolind, S., 2017. Cervical cord myelin water imaging shows degenerative changes over one year in multiple sclerosis but not neuromyelitis optica spectrum disorder. Neuroimage. Clin. 16, 17–22.

De Leener, B., Levy, S., Dupont, S.M., Fonov, V.S., Stikov, N., Louis Collins, D., Callot, V., Cohen-Adad, J., 2017. SCT: spinal cord toolbox, an open-source software for processing spinal cord MRI data. Neuroimage 145, 24–43.

De Leener, B., Fonov, V.S., Collins, D.L., Callot, V., Stikov, N., Cohen-Adad, J., 2018. PAM50: unbiased multimodal template of the brainstem and spinal cord aligned with the ICBM152 space. Neuroimage 165, 170–179.

Deoni, S.C.L., 2007. High-resolution T1 mapping of the brain at 3T with driven equilibrium single pulse observation of T1 with high-speed incorporation of RF field inhomogeneities (DESPOT1-HIFI). J. Magn. Reson. Imaging 26, 1106–1111.

Faizy, T.D., Thaler, C., Kumar, D., Sedlacik, J., Broocks, G., Grosser, M., Stellmann, J.P., Heesen, C., Fiehler, J., Siemonsen, S., 2016. Heterogeneity of multiple sclerosis lesions in multislice myelin water imaging. PLoS ONE 11.

Feldman, H.M., Yeatman, J.D., Lee, E.S., Barde, L.H., Gaman-Bean, S., 2010. Diffusion tensor imaging: a review for pediatric researchers and clinicians. J. Dev. Behav. Pediatr. 31, 346–356.

Gatto, R.G., 2018. Diffusion tensor imaging as a tool to detect presymptomatic axonal degeneration in a preclinical spinal cord model of amyotrophic lateral sclerosis. Neural Regen. Res. 13, 425–426.

Gros, C., De Leener, B., Badji, A., Maranzano, J., Eden, D., Dupont, S.M., Talbott, J., Ren, Z.Q., Liu, Y.O., Granberg, T., Ouellette, R., Tachibana, Y., Hori, M., Kamiya, K., Chougar, L., Stawiarz, L., Hillert, J., Bannier, E., Kerbrat, A., Edan, G., Labauge, P., Callot, V., Pelletier, J., Audoin, B., Rasoanandrianina, H., Brisset, J.C., Valsasina, P., Rocca, M.A., Filippi, M., Bakshi, R., Tauhid, S., Prados, F., Yiannakas, M., Kearney, H., Ciccarelli, O., Smith, S., Treaba, C.A., Mainero, C., Lefeuvre, J., Reich, D.S., Nair, G., Auclair, V., McLaren, D.G., Martin, A.R., Fehlings, M.G., Vandat, S., Khatibi, A., Doyon, J., Shepherd, T., Charlson, E., Narayanan, S., Cohen-Adad, J., 2019. Automatic segmentation of the spinal cord and intramedullary multiple sclerosis lesions with convolutional neural networks. Neuroimage 184, 901–915.

Harkins, K.D., Xu, J., Dula, A.N., Li, K., Valentine, W.M., Gochberg, D.F., Gore, J.C., Does, M.D., 2016. The microstructural correlates of T1 in white matter. Magn. Reson. Med. 75, 1341–1345.

Jeantroux, J., Kremer, S., Lin, X.Z., Collongues, N., Chanson, J.B., Bourre, B., Fleury, M., Blanc, F., Dietemann, J.L., de Seze, J., 2012. Diffusion tensor imaging of normal-appearing white matter in neuromyelitis optica. J. Neuroradiol. 39, 295–300.

Jeong, I.H., Choi, J.Y., Kim, S.H., Hyun, J.W., Joung, A., Lee, J.H., Kim, H.J., 2016. Comparison of myelin water fraction values in periventricular white matter lesions between multiple sclerosis and neuromyelitis optica spectrum disorder. Mult. Scler. J. 22, 1616–1620.

Jeong, I.H., Choi, J.Y., Kim, S.H., Hyun, J.W., Joung, A., Lee, J., Kim, H.J., 2017. Normal-appearing white matter demyelination in neuromyelitis optica spectrum disorder. Eur. J. Neurol. 24, 652–658.

Kearney, H., Miller, D.H., Ciccarelli, O., 2015. Spinal cord MRI in multiple sclerosis–diagnostic, prognostic and clinical value. Nat. Rev. Neurol. 11, 327–338.

Klawiter, E.C., Xu, J.Q., Naismith, R.T., Benzinger, T.L.S., Shimony, J.S., Lancia, S., Snyder, A.Z., Trinkaus, K., Song, S.K., Cross, A.H., 2012. Increased radial diffusivity in spinal cord lesions in neuromyelitis optica compared with multiple sclerosis. Mult. Scler. J. 18, 1259–1268.

Kolind, S.H., Deoni, S.C., 2011. Rapid three-dimensional multicomponent relaxation imaging of the cervical spinal cord. Magn. Reson. Med. 65, 551–556.

Kolind, S., Matthews, L., Johansen-Berg, H., Leite, M.I., Williams, S.C., Deoni, S., Palace, J., 2012. Myelin water imaging reflects clinical variability in multiple sclerosis. Neuroimage 60, 263–270.

Kolind, S., Sharma, R., Knight, S., Johansen-Berg, H., Talbot, K., Turner, M.R., 2013. Myelin imaging in amyotrophic and primary lateral sclerosis. Amyotroph Lateral Scler Frontotemporal Degener 14, 562–573.

Kolind, S., Seddigh, A., Combes, A., Russell-Schulz, B., Tam, R., Yogendrakumar, V., Deoni, S., Sibtain, N.A., Traboulsee, A., Williams, S.C., Barker, G.J., Brex, P.A., 2015. Brain and cord myelin water imaging: a progressive multiple sclerosis biomarker. Neuroimage Clin. 9, 574–580.

Kozlowski, P., Raj, D., Liu, J., Lam, C., Yung, A.C., Tetzlaff, W., 2008. Characterizing white matter damage in rat spinal cord with quantitative MRI and histology. J. Neurotrauma 25, 653–676.

Krampla, W., Aboul-Enein, F., Jecel, J., Lang, W., Fertl, E., Hruby, W., Kristoferitsch, W., 2009. Spinal cord lesions in patients with neuromyelitis optica: a retrospective long-term MRI follow-up study. Eur. Radiol. 19, 2535–2543.

Kurtzke, J.F., 1983. Rating neurologic impairment in multiple sclerosis: an expanded disability status scale (EDSS). Neurology 33, 1444–1452.
Laule, C., MacKay, A.L., 2014. Chapter 3.5 - T2 relaxation. In: Cohen-Adad, J., Wheeler-Kingshott, C. (Eds.), Quantitative MRI of the Spinal Cord. Academic Press.
Laule, C., Vavasour, I.M., Moore, G.R.W., Oger, J., Li, D.K.B., Paty, D.W., MacKay, A.L., 2004. Water content and myelin water fraction in multiple sclerosis - a T-2 relaxation study. J. Neurol. 251, 284–293.
Laule, C., Leung, E., Li, D.K.B., Troboulsee, A.L., Paty, D.W., MacKay, A.L., Moore, G.R.W., 2006. Myelin water imaging in multiple sclerosis: quantitative correlations with histopathology. Mult. Scler. 12, 747–753.
Laule, C., Kozlowski, P., Leung, E., Li, D.K.B., MacKay, A.L., Moore, G.R.W., 2008. Myelin water imaging of multiple sclerosis at 7 T: correlations with histopathology. Neuroimage 40, 1575–1580.
Laule, C., Vavasour, I.M., Zhao, Y., Traboulsee, A.L., Oger, J., Vavasour, J.D., Mackay, A.L., Li, D.K., 2010. Two-year study of cervical cord volume and myelin water in primary progressive multiple sclerosis. Mult. Scler. 16, 670–677.
Liu, H.W., MacMillian, E.L., Jutzeler, C.R., Ljungberg, E., MacKay, A.L., Kolind, S.H., Madler, B., Li, D.K.B., Dvorak, M.F., Curt, A., Laule, C., Kramer, J.L.K., 2017. Assessing structure and function of myelin in cervical spondylotic myelopathy evidence of demyelination. Neurology 89, 602–610.
Ljungberg, E., Vavasour, I., Tam, R., Yoo, Y., Rauscher, A., Li, D.K., Traboulsee, A., MacKay, A., Kolind, S., 2016. Rapid myelin water imaging in human cervical spinal cord. Magn. Reson. Med. 78 (4), 1482–1487.
MacKay, A., Whittall, K., Adler, J., Li, D., Paty, D., Graeb, D., 1994. In vivo visualization of myelin water in brain by magnetic resonance. Magn. Reson. Med. 31, 673–677.
MacKay, A., Laule, C., Vavasour, I., Bjarnason, T., Kolind, S., Madler, B., 2006. Insights into brain microstructure from the T-2 distribution. Magn. Reson. Imaging 24, 515–525.
MacMillan, Erin L., Madler, Burkhard, Fichtner, Nicole, Dvorak, Marcel F., Li, David K.B., Curt, Armin, MacKay, Alex L., 2011. Myelin water and T2 relaxation measurements in the healthy cervical spinal cord at 3.0T: repeatability and changes with age. Neuroimage 54, 1083–1090.
Manogaran, P., Vavasour, I., Borich, M., Kolind, S.H., Lange, A.P., Rauscher, A., Boyd, L., Li, D.K.B., Traboulsee, A., 2016. Corticospinal tract integrity measured using transcranial magnetic stimulation and magnetic resonance imaging in neuromyelitis optica and multiple sclerosis. Mult. Scler. J. 22, 43–50.
Martin, A.R., Aleksanderek, I., Cohen-Adad, J., Tarmohamed, Z., Tetreault, L., Smith, N., Cadotte, D.W., Crawley, A., Ginsberg, H., Mikulis, D.J., Fehlings, M.G., 2016. Translating state-of-the-art spinal cord MRI techniques to clinical use: a systematic review of clinical studies utilizing DTI, MT, MWF, MRS, and fMRI. Neuroimage-Clin. 10, 192–238.
Minty, E.P., Bjarnason, T.A., Laule, C., MacKay, A.L., 2009. Myelin water measurement in the spinal cord. Magn. Reson. Med. 61, 883–892.
Moreland, K., 2009. Diverging color maps for scientific visualization. In: Advances in Visual Computing, Pt 2, Proceedings. vol. 5876. pp. 92–103.
Muller, H.P., Gorges, M., Kassubek, R., Dorst, J., Ludolph, A.C., Kassubek, J., 2018. Identical patterns of cortico-efferent tract involvement in primary lateral sclerosis and amyotrophic lateral sclerosis: a tract of interest-based MRI study. Neuroimage Clin. 18, 762–769.
Nair, G., Carew, J.D., Usher, S., Lu, D., Hu, X.P.P., Benatar, M., 2010. Diffusion tensor imaging reveals regional differences in the cervical spinal cord in amyotrophic lateral sclerosis. Neuroimage 53, 576–583.
Nakamura, M., Miyazawa, I., Fujihara, K., Nakashima, I., Misu, T., Watanabe, S., Takahashi, T., Itoyama, Y., 2008. Preferential spinal central gray matter involvement in neuromyelitis optica - an MRI study. J. Neurol. 255, 163–170.
Nickerson, J.P., Koski, C.J., Boyer, A.C., Burbank, H.N., Tandan, R., Filippi, C.G., 2009. Linear longitudinal decline in fractional anisotropy in patients with amyotrophic lateral sclerosis: preliminary results. Klin. Neuroradiol. 19, 129–134.
Nijeholt, G.J., van Walderveen, M.A., Castelijns, J.A., van Waesberghe, J.H., Polman, C., Scheltens, P., Rosier, P.F., Jongen, P.J., Barkhof, F., 1998. Brain and spinal cord abnormalities in multiple sclerosis. Correlation between MRI parameters, clinical subtypes and symptoms. Brain 121 (Pt 4), 687–697.
Oh, J., Han, E.T., Lee, M.C., Nelson, S.J., Pelletier, D., 2007. Multislice brain myelin water fractions at 3T in multiple sclerosis. J. Neuroimaging 17, 156–163.
Pessoa, F.M., Lopes, F.C., Costa, J.V., Leon, S.V., Domingues, R.C., Gasparetto, E.L., 2012. The cervical spinal cord in neuromyelitis optica patients: a comparative study with multiple sclerosis using diffusion tensor imaging. Eur. J. Radiol. 81, 2697–2701.
Prasloski, T., Madler, B., Xiang, Q.S., MacKay, A., Jones, C., 2012a. Applications of stimulated echo correction to multicomponent T2 analysis. Magn. Reson. Med. 67, 1803–1814.
Prasloski, T., Rauscher, A., MacKay, A.L., Hodgson, M., Vavasour, I.M., Laule, C., Madler, B., 2012b. Rapid whole cerebrum myelin water imaging using a 3D GRASE sequence. Neuroimage 63, 533–539.
Pringle, C.E., Hudson, A.J., Munoz, D.G., Kiernan, J.A., Brown, W.F., Ebers, G.C., 1992. Primary lateral sclerosis - clinical-features, neuropathology and diagnostic-criteria. Brain 115, 495–520.
Qian, Wenshu, Chan, Queenie, Mak, Henry, Zhang, Zhongping, Anthony, Marina-Portia, Yau, Kelvin Kai-Wing, Khong, Pek-Lan, Chan, Koon Ho, Kim, Mina, 2011. Quantitative assessment of the cervical spinal cord damage in neuromyelitis optica using diffusion tensor imaging at 3 tesla. J. Magn. Reson. Imaging 33, 1312–1320.
Rivero, R.L.M., Oliveira, E.M.L., Bichuetti, D.B., Gabbai, A.A., Nogueira, R.G., Abdala, N., 2014. Diffusion tensor imaging of the cervical spinal cord of patients with Neuromyelitis Optica. Magn. Reson. Imaging 32, 457–463.
Simon, N.G., Turner, M.R., Vucic, S., Al-Chalabi, A., Shefner, J., Lomen-Hoerth, C., Kiernan, M.C., 2014. Quantifying disease progression in amyotrophic lateral sclerosis. Ann. Neurol. 76, 643–657.
Stroman, P.W., Wheeler-Kingshott, C., Bacon, M., Schwab, J.M., Bosma, R., Brooks, J., Cadotte, D., Carlstedt, T., Ciccarelli, O., Cohen-Adad, J., Curt, A., Evangelou, N., Fehlings, M.G., Filippi, M., Kelley, B.J., Kollias, S., Mackay, A., Porro, C.A., Smith, S., Strittmatter, S.M., Summers, P., Tracey, I., 2014. The current state-of-the-art of spinal cord imaging: methods. NEUROIMAGE 84, 1070–1081.
Vargas, W.S., Monohan, E., Pandya, S., Raj, A., Vartanian, T., Nguyen, T.D., Rua, S.M.H., Gauthier, S.A., 2015. Measuring longitudinal myelin water fraction in new multiple sclerosis lesions. Neuroimage-Clinical 9, 369–375.
Wang, Y., Liu, L., Ma, L., Huang, X.S., Lou, X., Wang, Y.L., Wu, N.Z., Liu, T.F., Guo, X.G., 2014. Preliminary study on cervical spinal cord in patients with amyotrophic lateral sclerosis using MR diffusion tensor imaging. Acad. Radiol. 21, 590–596.
Whittall, K.P., MacKay, A.L., Graeb, D.A., Nugent, R.A., Li, D.K.B., Paty, D.W., 1997. In vivo measurement of T-2 distributions and water contents in normal human brain. Magn. Reson. Med. 37, 34–43.
Wingerchuk, D.M., Hogancamp, W.F., O'Brien, P.C., Weinshenker, B.G., 1999. The clinical course of neuromyelitis optica (Devic's syndrome). Neurology 53, 1107–1114.
Wood, 2018. QUIT: QUantitative imaging tools. J. Open Source Software 3.
Wu, Y.J., Alexander, A.L., Fleming, J.O., Duncan, I.D., Field, A.S., 2006. Myelin water fraction in human cervical spinal cord in vivo. J. Comput. Assist. Tomogr. 30, 304–306.
Yoo, Y.J., Prasloski, T., Vavasour, I., MacKay, A., Traboulsee, A.L., Li, D.K.B., Tam, R.C., 2015. Fast computation of myelin maps from MRI T-2 relaxation data using multicore CPU and graphics card parallelization. J. Magn. Reson. Imaging 41, 700–707.